# Spin-Assembled Nanolayer of a Hyperbranched Polymer on the Anode in Organic Light-Emitting Diodes: The Mechanism of Hole Injection and Electron Blocking

Tae-Woo Lee,*[‡] Jong-Jin Park,[‡] Young Kwon,[§] Teruaki Hayakawa,[§] Tae-Lim Choi,[‖]
Jong Hyeok Park,[⊥] Rupasree Ragini Das,[‡] and Masa-aki Kakimoto[§]

*Samsung Advanced Institute of Technology, Mt. 14-1, Nongseo-dong, Giheung-gu, Yongin-si,
Gyeonggi-do 446-712, Korea, Department of Organic and Polymeric Materials, Tokyo Institute of
Technology, Tokyo 152-8550, Japan, Electronic Chemical Materials R&D Center, Cheil Industries Inc.,
332-2 Gogcheon-dong, Uiwang-si, Gyunggi-do 437-711, Korea, and Department of Chemical Engineering,
Sungkyunkwan University, Suwon 440-746, Korea*

We introduced a spin-assembled nanolayer of hyperbranched poly(ether sulfone) with sulfonic acid terminal on top of an indium−tin oxide anode in organic light-emitting diodes. This results in great improvement in luminous efficiency, better than that of devices using a commercially available conducting polymer composition as a hole-injection layer. The effect of the nanolayer was investigated by impedance spectroscopy, photovoltaic measurement for built-in-potential, and transient electroluminescence. We concluded that the high luminous efficiency resulted from the efficient electron-blocking by the nanolayer and hole-injection assisted by the accumulation of electrons at the interface. This result implies that, for an efficient hole-injection layer, the electron-blocking capability should be incorporated in addition to the hole-injection and -transport capability.

## Introduction

There have been several different approaches to improve the electronic charge balance for efficient radiative recombination by modifying the hole-injection contact.[1−13] Generally, to date, hole-injection layers (HIL), which can inject and transport holes from anode (such as indium−tin oxide (ITO)), have been incorporated in organic light-emitting diodes (OLEDs).[1−11] To design efficient HILs, the highest occupied molecular orbital level (HOMO) and the hole conductivity of the material are important parameters for hole-injection and -transport, respectively. In particular, the relative alignment of the HOMO levels of HILs at interfaces between ITO and the HIL or between the

HIL and overlying organic materials is crucial in order to understand the device physics of charge-carrier injection, transport, and radiative recombination. Arylamine derivatives such as 4,4′,4″-tris{*N*-(2-naphthyl)-*N*-phenylamino}triphenyl-amine (*m*-MTDATA)[10,11] and 4,4′,4″-tris{*N*-(2-naphthyl)-*N*-phenylamino}triphenylamine (2T-NATA)[10] have been frequently used for the hole-injection layer by vacuum deposition because the HOMO levels are located between ITO work function (4.7−4.9 eV) and HOMO levels of the overlying hole-transport layer [e.g., *N*,*N*′-dinaphthalen-1-yl-*N*,*N*′-diphenylbenzidine (NPB); HOMO ∼ −5.4 eV] or the emitting layers [e.g., tris(8-hydroxy-quinolato) aluminum (Alq₃); HOMO ∼ −5.7 eV]. Also their hole-transport mobilities are high enough (∼$10^{-4}$ cm²/V s)[14] for the efficient transport of holes from the ITO anode to the overlying layers. As for polymeric hole-injection layers, it has been well-known that conducting polymer films such as polyaniline,[2] polypyrrole,[3] and poly(3,4-ethylenedioxythiophene) (PEDOT)[4−7] on an indium tin oxide (ITO) layer play important roles to improve the device efficiency by enhancing the hole-injection from the ITO. Among them, the commercially available polymer HIL materials are Baytron P series from H. C. Starck, GmbH, which are composed of PEDOT and polystyrene sulfonate (PSS) in aqueous dispersion. These kinds of solution-processed polymeric HILs have an advantage over vacuum-deposited small molecule HILs in that the polymer layer can reduce the surface roughness of uneven ITO. However, since PEDOT:PSS aqueous dispersion has a large particle size (average ca. 60 nm),[15] controlling the

* Corresponding author. E-mail: twlee@postech.ac.kr. Current address: Department of Materials Science and Engineering, Pohang University of Science and Technology, Pohang, Gyungbuk 790-784, Korea.
　‡ Samsung Advanced Institute of Technology.
　§ Tokyo Institute of Technology.
　‖ Cheil Industries Inc. Current address: Department of Chemistry, Seoul National University, Seoul 151-742, Korea.
　⊥ Sungkyunkwan University.

(1) (a) Lee, T.-W.; Lee, H.-C.; Park, O. O. *Appl. Phys. Lett.* **2002**, *81*, 214. (b) Lee, T.-W.; Park, O. O. *Adv. Mater.* **2001**, *13*, 1274. (c) Lee, T.-W.; Park, O. O.; Kim, J.-J.; Hong, J.-M.; Kim, Y. C. *Chem. Mater.* **2001**, *13*, 2217. (d) Winroth, G.; Latini, G.; Credgington, D.; Wong, L.-Y.; Chua, L.-L.; Ho, P. K.-H; Cacialli, F. *Appl. Phys. Lett.* **2008**, *92*, 103308.
(2) (a) Yang, Y.; Westerweele, E.; Zhang, C.; Smith, P.; Heeger, A. J. *J. Appl. Phys.* **1995**, *77*, 694. (b) Higgins, R. W. T.; Zaidi, N. A.; Monkman, A. P. *Adv. Funct. Mater.* **2001**, *11*, 407. (c) Huh, D. H.; Chae, M.; Bae, W. J.; Jo, W. H.; Lee, T.-W. *Polymer* **2007**, *48*, 7236.
(3) Gao, J.; Heeger, A. J.; Lee, J. Y.; Kim, C. Y. *Synth. Met.* **1996**, *82*, 221.
(4) (a) Lee, T.-W.; Kwon, O.; Kim, M.-G.; Park, S. H.; Chung, J.; Kim, S. Y.; Chung, Y.; Park, J.-Y.; Han, E.; Huh, D. H.; Park, J.-J.; Pu, L. *Appl. Phys. Lett.* **2005**, *87*, 231106. (b) Lee, J. Y. *Chem. Phys. Lett.* **2004**, *393*, 260.
(5) (a) Park, J.; Kwon, Y.; Lee, T.-W. *Macromol. Rapid Commun.* **2007**, *28*, 1366. (b) Lee, T.-W.; Chung, Y.; Kwon, O.; Park, J.-J. *Adv. Funct. Mater.* **2007**, *17*, 390. (c) Lee, T.-W.; Chung, Y. *Adv. Funct. Mater.* **2008**, *18*, 2246.
(6) Carter, S. A.; Angelopoulos, M.; Karg, S.; Brock, P. J.; Scott, J. C. *Appl. Phys. Lett.* **1997**, *70*, 2067.
(7) Elschner, A.; Bruder, F.; Heuer, H.-W.; Jonas, F.; Karbach, A.; Kirchmeyer, S.; Thurm, S.; Wehrmann, R. *Synth. Met.* **2000**, *111–112*, 139.
(8) (a) Kato, S. *J. Am. Chem. Soc.* **2005**, *127*, 11538. (b) Lim, B.; Hwang, J.-T.; Kim, J. Y.; Ghim, J.; Vak, D.; Noh, Y.-Y.; Lee, S.-H.; Lee, K.; Heeger, A. J.; Kim, D.-Y. *Org. Lett.* **2006**, *8*, 4703.

(9) Ho, P. K. H.; Kim, J.-S.; Burroughes, J. H.; Becker, H.; Li, S. F. Y.; Brown, T. M.; Cacialli, F.; Friend, R. H. *Nature* **2000**, *404*, 481.
(10) Hamada, Y.; Matsusue, N.; Kanno, H.; Fujii, H. *Jpn. J. Appl. Phys.* **2001**, *40*, L753.
(11) Chen, S.; Wu, Z.; Zhao, Y.; Li, C.; Hou, J.; Liu, S. *Org. Electron.* **2005**, *6*, 111.
(12) Huang, Q.; Cui, J.; Yan, H.; Veinot, J. G. C.; Marks, T. J. *Appl. Phys. Lett.* **2002**, *81*, 3528.
(13) Nüesch, F.; Rothberg, L. J.; Forsythe, E. W.; Le, Q. T.; Gao, Y. *Appl. Phys. Lett.* **1999**, *74*, 880.
(14) Tse, S. C.; Kwok, K. C.; So, S. K. *Appl. Phys. Lett.* **2006**, *89*, 262102.

particle size for the good film quality without defect can be another issue for large-size panel displays. In addition, the film-forming process such as spin-coating cannot be conducted in an inert glovebox, because the composition is dispersed in water. As a result, organic-soluble hole-injection materials with a performance at least comparable to the conventional PEDOT: PSS dispersion are desired.

Here we introduce a spin-assembled nanolayer of hyper-branched poly(ether sulfone) with sulfonic acid terminal as a HIL instead of conventional conducting polymers. The thin insulating nanolayer on top of ITO acts as a good hole-injection layer as well as a electron-blocking layer, which gives more balanced electron−hole recombination in the OLED device. As a result, the luminous efficiency is better than the value we obtained from the device using conventional PEDOT:PSS as a hole-injection layer. Then, we investigated the effect of the nanolayer on the charge injection and transport by using photovoltaic measurement for built in potential, transient electroluminescence, and impedance spectroscopy. Here we focused on the role and the origin of the insulating nanolayer on ITO for its improved device performance. From this study, some insights on how to design novel HILs to improve the device efficiency can be obtained.

## Experimental Section

**Chemicals.** Toluene and nitrobenzene were dried with calcium hydride and then distilled under reduced pressure. All other chemicals are regent grade and were used as received unless otherwise stated.

**Chemical Analysis.** Infrared (IR) spectra were recorded on a Shimadzu FTIR-8100 Fourier transform infrared spectrophotometer. NMR spectra were recorded on a JEOL JNM-AL 300 MHz spectrometer. Thermogravimetric analysis (TGA) was carried out with a Seiko TG/DTA 6200 at a heating rate of 10 °C/min under air. Gel permeation chromatography (GPC) was performed on a Shodex RI-71 refractive index detector. Dimethylformamide (DMF) containing 0.01 M of lithium bromides was used as eluent.

**Preparation of Monomer, 4,4′-(*m*-Phenylenedioxy)bis(ben-zenesulfonyl chloride).[16]** To a 100-mL round-bottom flask equipped with a Dean−Stark apparatus and a reflux condenser were added sodium *p*-fluorobenzenesulfonate (2.9 g, 14 mmol), resorcinol (0.66 g, 6.0 mmol), potassium carbonate (2.5 g, 18 mmol), sulfolane (24 mL), and toluene (20 mL). The reaction mixture was heated to 150 °C for 2 h and then at 240 °C for 20 h and poured into dichloromethane. The precipitate was dissolved in hydrochloric acid solution. The filtrate was adjusted to pH 10 by adding sodium hydroxide solution. To this solution was added NaCl to precipitate 4,4′-(*m*-phenylenedioxy)bis(benzenesulfonicacid disodium salt). It was recrystallized from ethanol and water. This salt was treated with POCl₃ (3 mL) at 130 °C for 6 h. The reaction mixture was poured in ice−water and extracted with dichloromethane. The product was purified using column chromatography (with 3:2 hexane:dichloromethane solvent mixture) and was obtained as a viscous liquid. Yield: 1.58 g, 57%. IR (NaCl, cm⁻¹): 1184, 1377 (SO₂Cl), 1242 (Ar−O−Ar), 1477, 1577 cm⁻¹ (Ph-H). ¹H NMR (CDCl₃, ppm): 6.89 (s, 1H), 7.02 (d, 2H), 7.15 (d, 4H), 7.51 (t, 1H), 8.03 (d, 4H). Anal. Calcd (C₁₈H₁₂Cl₂O₆S₂): C; 47.07; H, 2.63. Found: C, 47.06; H, 2.79.

**Preparation of Hyperbranched Aromatic Poly(ether sulfone) with Sulfonyl Chloride Terminal Groups.[16]** A solution of 4,4′-(*m*-phenylenedioxy)bis(benzenesulfonyl chloride) (0.30 g, 0.65 mmol), nitrobenzene (2 mL), and FeCl₃ (0.003 g, 0.018 mmol) was stirred at 110 °C for 3 h. The solution was cooled to room temperature and poured into methanol containing a small amount of concentrated hydrochloric acid solution. The precipitate was washed with methanol and dried at 80 °C under vacuum; 0.23 g of the product was isolated with 88% yield. ¹H NMR (ppm): 8.4−6.4 (m), IR (KBr, cm⁻¹); 1184, 1376 (SO₂Cl), 1223 (Ar−O−Ar), 1473, 1577 cm⁻¹ (Ph-H).
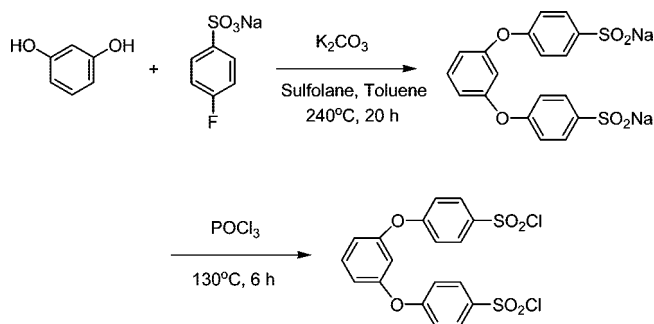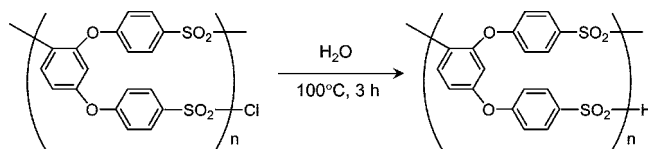


**Preparation of Hyperbranched Aromatic Poly(ether sulfone) with Sulfonyl Acid Terminal Groups.** In a 200 mL flask, 1 g of hyperbranched aromatic poly(ether sulfone) with sulfonyl chloride terminal groups was suspended in 120 mL of water. The mixture was refluxed for 3 h. After the water was evaporated, 0.89 g of the white product was collected. The structure of hyperbranched aromatic poly(ether sulfone) with sulfonyl acid terminal groups was determined by spectral analysis. ¹H NMR (ppm): 8.4−6.4 (m). IR (KBr, cm⁻¹): 1184, 1223 (Ar−O−Ar), 1473, 1577 cm⁻¹ (Ph−H). TGA: 365 °C (10% weight loss). GPC: $M_w = 31\,100$, $M_n = 19\,100$, PDI = 1.62.
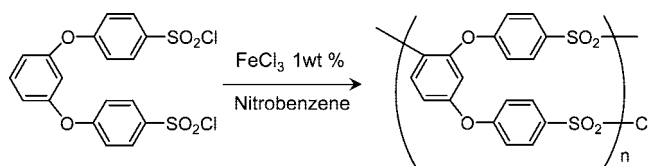


**OLEDs Fabrication and Characterization.** The HB-PES dissolved in dimethylformamide and PEDOT:PSS dispersed in water (Baytron P VP AI4083, H. C. Starck GmbH) were spin-coated on top of UV/ozone treated ITO in a N₂-filled glovebox and in air and gave 4.37 and 60 nm films, respectively. The films were baked on a hot plate in the N₂-filled glovebox at 130 °C for 30 min and 200 °C for 10 min. A bare ITO without the HIL layers was treated by UV/ozone just before loading the substrates into the vacuum chamber to prevent the change of the UV/ozone-treated ITO surface. A green-emitting Alq₃ (LumTec Corp.) was deposited by vacuum evaporation to obtain 60 nm thickness under vacuum below $3 \times 10^{-7}$ Torr. The 1 nm LiF and 150 nm Al were sequentially deposited on the emitting layer under vacuum below $5 \times 10^{-7}$ Torr. The OLED devices were encapsulated with a glass lid by using a epoxy resin. The $I-V-L$ characteristics were obtained with a Keithley 238 source-measure unit and a Photo Research PR650 spectropho-tometer. The capacitance−voltage measurement was performed by using impedance analyzer (Solartron 1260).

**Photovoltaic and Capacitance Measurement.** The OLEDs were cycled two times between −4 and 4 V to ensure reproducible operation of their current in the absence of microscopic shorts. For the photovoltaic measurements, a mercury lamp (Blak-Ray, 100 W bulb, 365 nm, 7 mW/cm² at 38 cm) was used for illumination and a Solartron SI 1287 potentiostat was used to record the electrical characteristics. For each cycle, the voltages between −4 and 4 V were sourced with 50 mV step size and 1 s step time and the dark current density was measured. Then, the sample was allowed to relax for ca. 20 s, and subsequently, current density under illumination was measured. The capacitance versus voltage characteristics were measured while dc voltages were applied from −4 to 4 V at ac frequency of 100 Hz and ac amplitude of 50 mV by a Solartron SI 1260 impedance/gain-phase analyzer.



**Transient Electroluminescence Measurement.** For transient EL measurements, a low duty cycle electrical pulse (100 μs pulse width,

**Scheme 1. Synthesis of Hyperbranched Aromatic Poly(ether sulfone) with Sulfonic Acid Terminal Groups (HB-PES)**
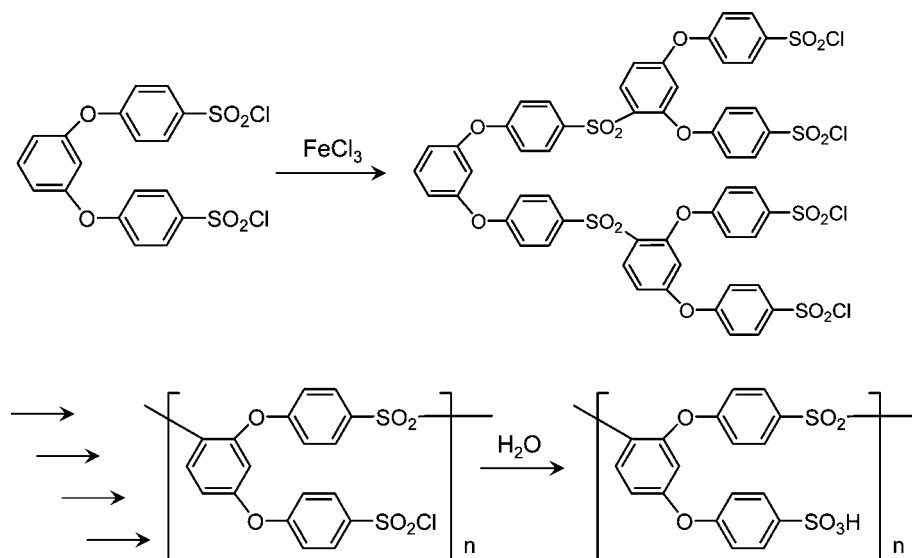


10 Hz pulse frequency) from a pulse/function generator (HP 8116A 50 MHz) was applied to the device. The low duty cycle of the electrical pulses can minimize any device heating and reduce the residual space charges after every turn-off of the voltage pulse. The emitted light was detected by a photomultiplier tube assembly (HC125-01, Hamamatsu Corp., rise time of 1.5 ns). The pulse shape and the photodetector output signal were measured by an oscilloscope (Agilent Infinium 54830B oscilloscope 600 MHz 4 GSa/s).

## Results and Discussion

Hyperbranched polymers are interesting new materials with their unique properties, such as inherent globular structure, low viscosity, high solubility, and large number of terminal functional groups, which will be advantageous for solution process to form thin films on substrates. Scheme 1 shows the synthetic scheme for hyperbranched poly(ether sulfone) with sulfonic acid terminal (HB-PES). The synthetic scheme of HB-PES is described in the Experimental Section in detail. The material has a good adhesion to the ITO surface due to the presence of a large number of sulfonic acid end groups, so simple spin-coating generates a thin homogeneous nanolayer film. This sulfonic acid group can shift the common vacuum level upward.[13] Previously, it was reported that the chemical adsorption of acids such as sulfonic acid and phosphoric acid increases the work function of ITO owing to a double ionic surface layer.[13] In this case, dipoles near the electrodes create a drop in energy barrier at the interface given by $\Delta\Phi = Fd = \sigma d/\varepsilon_o\varepsilon = N\mu/\varepsilon_o\varepsilon$, for an applied field $F$, where $d$ is the distance between positive and negative partial charges, $\varepsilon_o$ is the permittivity of vacuum, $\varepsilon$ is the static dielectric constant, $\sigma$ is the surface charge density, $N$ is the number of charges per unit surface, and $\mu$ is the dipole moment.[17] As a result, the hole-injection can be enhanced.

On the other hand, the HB-PES is electrically insulating, so the layer can block the electrons at the interface. Therefore, the

layer performs two different functions, hole-injection and electron-blocking. In the previous literatures, ultrathin layers of insulating inorganic materials such as $SiO_2$,[18a] $Pr_2O_3$,[18b] $WO_3$,[18c] and $LiF$[18d] have been deposited on ITO to enhance the hole-injection and electron-blocking for better electron–hole balance. In these reports, the optimum thickness for the best luminous efficiency turned out to be around 5–10 Å. However, it is difficult to form the uniform monolayer of the insulating inorganic materials on ITO with only 5–10 Å thickness, and thus, thickness control for practical mass production of devices will be a very critical issue. Instead, casting a homogeneous thin organic layer on ITO can be an alternative solution due to the simple solution process without using a vacuum process. It was reported that the modification of the ITO surface with an ultrathin (1–2 nm) self-assembled organosiloxane hydrocarbon monolayer can enhance not only the hole-injection and electron-blocking but also the device efficiency.[12] However, these materials need special care, because they are very reactive in the presence of moisture. Therefore, we propose that the simple and low-cost material of HB-PES can be utilized as a hole-injection and electron-blocking layer by forming a homogeneous thin layer on ITO. A previous study showed that acid–based self-assembled monolayer (SAM) dielectric was densely packed, resulting in a great reduction in the leakage current through the monolayer versus that of the device without the SAM and even much smaller than that of the device with silane-based SAM.[19] Therefore, the sulfonic acid terminated HB-PES layer can be advantageous as hole-injection buffer film on the anode in PLEDs.

To obtain a very thin nanolayer film of the HB-PES, 0.5 wt % HB-PES solution in DMF was spin-coated on top of a silicon wafer treated with ultraviolet (UV)/ozone at a high spin speed of 4000 rpm. The cast film was characterized by a small-angle X-ray reflectivity measurement, which was performed with Cu Kα radiation ($\lambda = 1.542$ Å) at room temperature by using a Phillips X'pert Pro PW3040 diffractometer. The experimental reflectivity curve was analyzed by the Wingixa program according to the Parratt algorithm.[20] The measured reflectivity curve along with the curve fit is shown in Figure 1. The X-ray reflectivity spectrum clearly shows the Kiessig oscillations due to the interference of beams reflected from the upper and the lower

(15) The information is available in the H.C. Starck website, http://www.hcstarck.com/.

(16) Matsumoto, K.; Ueda, M. *Chem. Lett.* **2006**, *35*, 1196.

(17) Lee, T.-W.; Zaumseil, J.; Kim, S. H.; Hsu, J. W. P. *Adv. Mater.* **2004**, *16*, 2040.

(18) (a) Deng, Z. B.; Ding, X. M.; Lee, S. T.; Gambling, W. A. *Appl. Phys. Lett.* **1999**, *74*, 2227. (b) Qiu, C.; Chen, H.; Xie, Z.; Wong, M.; Kwok, H. S. *Appl. Phys. Lett.* **1999**, *80*, 3485. (c) Li, J.; Yahiro, M.; Ishida, K.; Yamada, H.; Matsushige, K. *Synth. Met.* **2005**, *151*, 141. (d) Zhu, F. R.; Low, B. L.; Zhang, K. R.; Chua, S. J. *Appl. Phys. Lett.* **2001**, *79*, 1205.

(19) Klauk, H.; Zchieschang, U.; Pflaum, J.; Halik, M. *Nature* **2007**, *445*, 745.

(20) Parratt, L. G. *Phys. Rev.* **1954**, *95*, 359.
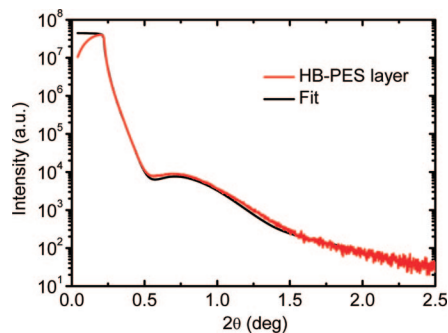
**Figure 1.** Small angle X-ray reflectivity: measurement data and curve fit (obtained according to the Parratt algorithm).

interfaces, indicating that the layer has a smooth surface (rms $\sim$ 9 Å). The value obtained for the thickness of the HB-PES layer is 43.7 Å.

To investigate the roles of HB-PES, three different OLEDs with a single $Alq_3$ layer were fabricated as follows (see Figure 2): (i) $ITO/Alq_3/LiF/Al$, (ii) $ITO/HB-PES/Alq_3/LiF/Al$, (iii) $ITO/PEDOT:PSS/Alq_3/LiF/Al$. The reason why we chose single-layer devices instead of state-of-the-art multilayer devices is that these single-layer OLED devices can clearly show the effect of only the HB-PES layer on charge injection and transport as reported in the previous literature.[21,22] The ITO anode was treated with UV/ozone for 15 min, followed by spin-coating a 60 nm thick PEDOT:PSS. $Alq_3$ was vacuum deposited on top of these layers as an emitting layer under a vacuum of $1 \times 10^{-7}$ Torr. Finally, LiF (1 nm)/Al (150 nm) was deposited by thermal evaporation under a vacuum of $3 \times 10^{-7}$ Torr.

We first investigated the current$-$voltage$-$luminance ($I-V-L$) characteristics of the OLED devices using the HB-PES layer. When we introduced the HB-PES nanolayer on top of ITO in $Alq_3$-based devices, the current density was reduced compared with those devices without using the layer, as shown in Figure 2b. On the contrary, the device using PEDOT:PSS layer showed a little increase in current density because the hole-injection is enhanced by the PEDOT:PSS layer. In $Alq_3$-based devices, electrons are more dominant than holes, so the total current densities are mostly influenced by electron current. Therefore, the large reduction on current densities of the device using the HB-PES layer can be attributed to the efficient electron-blocking capability of HB-PES layer. The HB-PES device showed higher luminous, power, and quantum efficiency (3.2 cd/A, 2.8 lm/W, and 1.2% ph/el) than the PEDOT:PSS device (1.7 cd/A, 1.26 lm/W, and 0.63% ph/el) despite the reduced current density, as Figure 2c,d shows. This implies that the HB-PES layer blocks electrons better than the PEDOT:PSS layer, and thus, the electron$-$hole balance for radiative recombination is improved. Also previous literature reports that the PEDOT:PSS layer can quench the radiative excitons in the device,[23] whereas HB-PES does not quench the excitons, leading to the increase in the luminous efficiency. The luminous efficiency of our simple device (3.2 cd/A) was comparable to multilayer devices of $ITO/NPB/Alq_3/LiF/Al$ reported elsewhere[24,25] (ca. 2.0 cd/A in ref 24, ca. 3.5 cd/A in ref 25).

We performed a photovoltaic measurement of the built-in potential in the OLED devices to investigate the work function
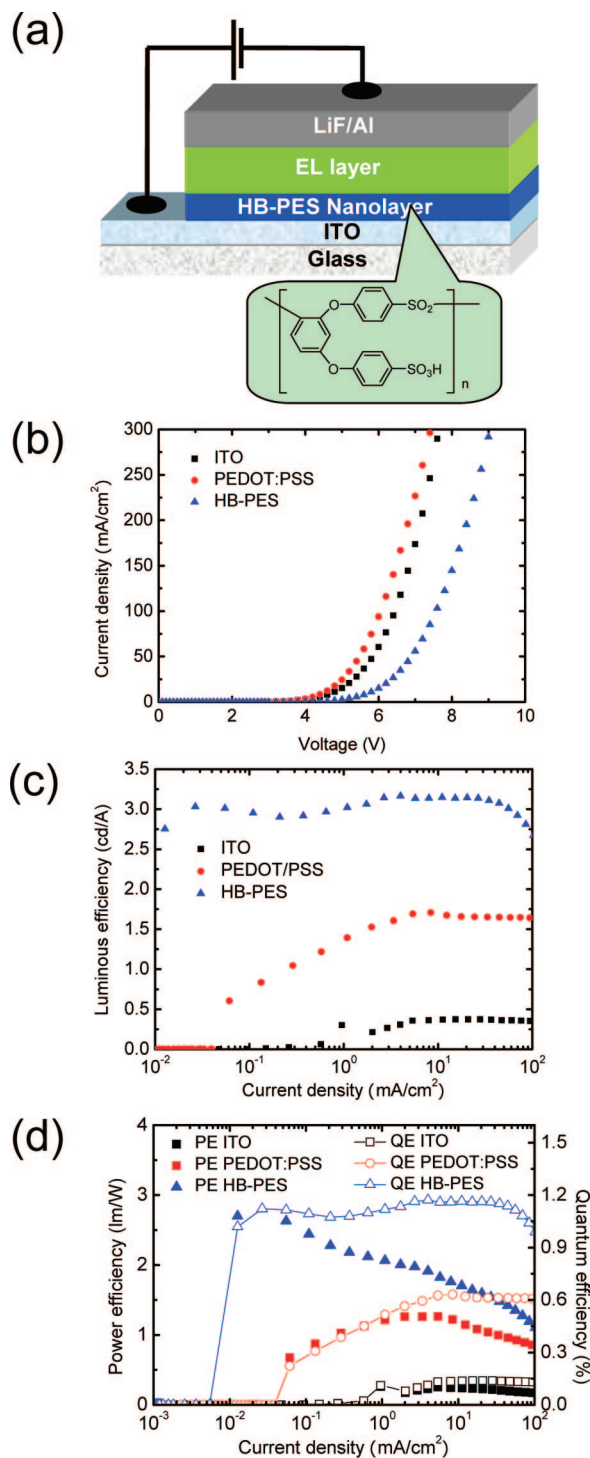


**Figure 2.** (a) The device structure of a single-layer $Alq_3$ device using HB-PES as a hole-injecting and electron-blocking layer. (b) Current density versus voltage, (c) luminous efficiency versus current density, and (d) power efficiency and quantum efficiency versus current density characteristics of three different single-layer $Alq_3$ devices using ITO, PEDOT:PSS/ITO, and HB-PES/ITO. The bare ITO substrate was treated with UV/ozone just before loading the samples into the vacuum chamber.

change of the anode contact by the HB-PES layer (Figure 3)[26] This estimate is only tentative and will need to be confirmed by

(21) Blochwitz, J.; Pfeiffer, M.; Fritz, T.; Leo, K. *Appl. Phys. Lett.* **1998**, *73*, 729.
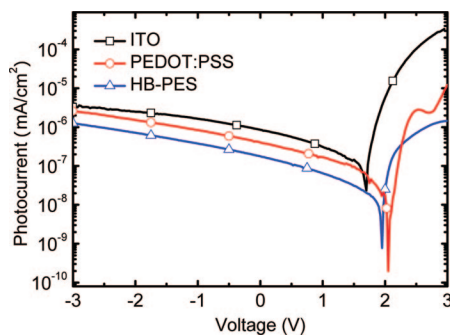
(22) Zhou, X.; Blochwitz, J.; Pfeiffer, M.; Nollau, A.; Fritz, T.; Leo, K. *Adv. Funct. Mater.* **2001**, *11*, 310.

(23) Kim, J.-S.; Friend, R. H.; Grizzi, I.; Burroughes, J. H. *Appl. Phys. Lett.* **2005**, *87*, 023506.

(24) Xie, W.; Zhang, L.; Liu, S. *Semicond. Sci. Technol.* **2004**, *19*, 380.

(25) Forsythe, E. W.; Abkowitz, M. A.; Gao, Y. *J. Phys. Chem. B* **2000**, *104*, 3948.

(26) Malliaras, G. G.; Salem, J. R.; Brock, P. J.; Scott, J. C. *J. Appl. Phys.* **1998**, *84*, 1583.

**Figure 3.** Absolute photocurrent versus voltage characteristics of the single-layer $Alq_3$ devices using ITO, PEDOT:PSS/ITO, and HB-PES/ITO.



**Figure 4.** Capacitance versus voltage characteristics of the single-layer $Alq_3$ devices using ITO, PEDOT:PSS/ITO, and HB-PES/ITO. Data were obtained while dc voltages from $-4$ to 4 V at ac frequency of 100 Hz and ac amplitude of 50 mV were applied by an impedance/gain-phase analyzer.

more accurate methods/determinations, such as the electroabsorption spectroscopy of the devices or ultraviolet photoelectron spectroscopy (UPS). Therefore, we also measured the work functions of the ITO, the PEDOT:PSS/ITO, and the HB-PES/ITO by using UPS. Although many attempts were made to measure the work function of the HB-PES modified ITO by UPS in air (surface analyzer, model AC2, Riken Keiki Co. Ltd.), we failed because the photoelectron signal was so weak due to the insulating nature of the HB-PES films preventing the photoelectrons from escaping out of the layer. As an alternative, the photovoltaic measurement can be effective for estimating the work function shift of the electrodes modified by an insulating material.

We measure the voltage at which the current under illumination in $Alq_3$-based light-emitting diodes is equal to the dark current (i.e., the net photocurrent is zero). In principle, the voltage corresponds to the built-in potential of the OLEDs in the absence of diffusive transport of charges. The built-in potential measured at low temperature can give a good estimation of the work function of the anode and cathode contacts in the rigid-band approximation.[26] Since we measured the voltage where the net photocurrent is zero at room temperature (here called $V_{BI}$), we are focusing on the relative changes of the work function of HB-PES modified ITO compared with the bare ITO and the PEDOT:PSS/ITO. The $V_{BI}$ of $ITO/Alq_3/LiF/Al$ and $ITO/PEDOT:PSS/Alq_3/LiF/Al$ devices were 1.70 and 2.05 eV, respectively. UPS (AC2) measurement gave the work function of 4.85 and 5.20 eV for ITO and PEDOT-PSS, respectively. In the rigid band approximation, the built-in potential is determined from the work function difference between ITO and the cathode. Therefore, the effective work function of LiF/Al can be calculated as 3.15 eV when we subtract 1.70 eV ($V_{BI}$) from 4.85 eV (the ITO work function). As for the devices using PEDOT:PSS on top of ITO, the built-in potential is determined by the difference of work function between PEDOT:PSS and the cathode.[27] The estimated effective work function of LiF/Al cathode also becomes 3.15 eV when we subtract 2.05 eV ($V_{BI}$) from 5.20 eV (PEDOT:PSS work function). The value (3.15 eV) is a little higher than the value (2.95 eV) estimated using the built-in potential (1.8 eV for 0.9 nm LiF) by electroabsorption spectroscopy.[28] Although the cathode work function estimated from the photovoltaic method is tentative, we can use the effective value of 3.15 eV to extract the anode work function of HB-PES/ITO, which turns out to be 5.10 eV. The literature reports that the adsorption of positively charged poly(amidoamine) dendrimers on the ITO surface resulted
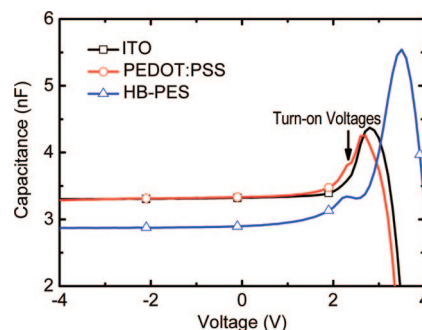
in significant lowering (0.55 eV) of the effective work function.[29] However, since the spin-cast HB-PES is negatively charged, the effective work function can be increased.

From these measurements, we find that the hole-injection is more facilitated compared with the device without using the HB-PES layer. The holes can be injected through the insulating layer via tunneling because the layer is thin enough. On the other hand, the device using the PEDOT:PSS layer has better hole-injection capability than the HB-PES layer, since the work function of PEDOT:PSS is higher (5.20 eV). Despite this result, the device using the HB-PES layer showed better luminous efficiency than the device using the PEDOT-PSS layer. We attribute this to the efficient electron-blocking of the HB-PES layer at the HB-PES/$Alq_3$ interface. As a result, electron accumulation at the interface induces more hole-injection from the anode, which will be supported by impedance spectroscopy and transient electroluminescence as follows.

To investigate the effect of the accumulated electrons at the interface on the device, we measured capacitance−voltage characteristics by an ac impedance analyzer (Solartron 1260), as Figure 4 shows. The capacitance in reverse biases is almost constant. The sharp increase in the capacitance above 2 V is observed. The capacitance continues to increase up to the device turn-on voltages ($\sim$2.5 V) where electron−hole recombination starts to take place. This process corresponds to the majority carrier injection and accumulation. The voltages with the shoulder capacitance peaks correspond to the device turn-on voltages at which light-emission from the emitting layer begins. Then, the minority carriers (holes) start to be injected and then recombine with electrons. The main capacitance peaks correspond to the voltage points where electrons are accumulated most without recombination. After these voltages, the capacitance tends to decrease drastically due to the electron−hole recombination.[30] The capacitance (3.33 nF) before the majority charge injection for the device using the PEDOT:PSS layer was almost identical to that for the device (3.32 nF) without using the PEDOT:PSS layer. Since PEDOT:PSS is much more conducting than $Alq_3$, the electric field is applied only to the $Alq_3$, despite the thick PEDOT:PSS layer. However, when the HB-PES thin nanolayer was incorporated instead, the capacitance of the device before the majority charge injection slightly decreased to 2.90 nF. This implies that the electric field for this device is applied to both the HB-PES layer and the $Alq_3$ layer at the same time. The maximum capacitance after the turn-on voltage for the device

(27) Brown, T. M.; Kim, J. S.; Friend, R. H.; Cacialli, F.; Daik, R.; Feast, W. J. *Appl. Phys. Lett.* **1999**, *75*, 1679.
(28) Brown, T. M.; Friend, R. H.; Millard, I. S.; Lacey, D. J.; Burroughes, J. H.; Cacialli, F. *Appl. Phys. Lett.* **1999**, *75*, 1679.

(29) Latini, G.; Wykes, M.; Schlapak, R.; Howorka, S.; Cacialli, F. *Appl. Phys. Lett.* **2008**, *92*, 013511.
(30) Shrotriya, V.; Yang, Y. *J. Appl. Phys.* **2005**, *97*, 054504.
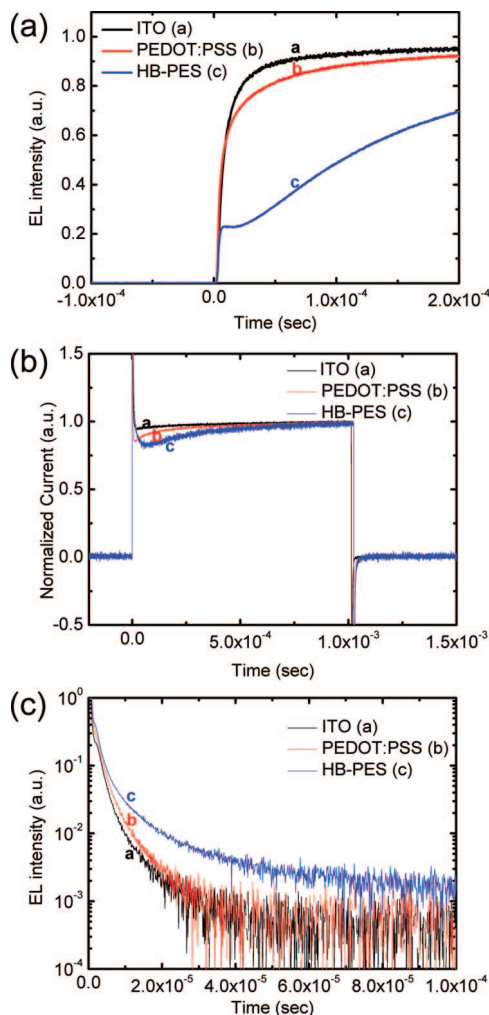
**Figure 5.** Transient current and electroluminescence characteristics of the single-layer $Alq_3$ devices using ITO, PEDOT:PSS/ITO, and HB-PES/ITO. (a) Transient electroluminescence rising curves, (b) transient current curves, and(c) transient electroluminescence decay curves. A low duty cycle electrical pulse ($100\,\mu$s pulse width, 10 Hz pulse frequency) from a pulse/function generator was applied to the device.

using the HB-PES is much higher than that without it. This implies that the electrons are accumulated more at the HB-PES/$Alq_3$ interface than at PEDOT:PSS/$Alq_3$ and ITO/$Alq_3$ interfaces before radiative recombination takes places.

We performed transient electroluminescence (EL) measurements to observe if the accumulated electrons can induce more holes from the ITO anode. We observed transient EL of three different OLEDs with 6 V step voltage pulse and 10 Hz frequency, as shown in Figure 5. We observed the delay time (i.e., light onset time, $t_d$), the rising time (i.e., light saturation time, $t_r$), and the decay time after turn-off. The delay times for the three different $Alq_3$ devices with ITO, PEDOT:PSS/ITO, and HB-PES/ITO anodes were 2.53, 2.38, and 2.53 $\mu$s, respectively. Since the current of the EL devices is electron dominant, the delay time is almost unchanged. We defined the rising time as the time required to reach 95% of the maximum light intensity after switch-on. Since the rising time corresponds to how fast the hole−electron recombination reaches the steady state, the $t_r$ is controlled by the minority carriers (or holes) in the devices. The $t_r$ values for the three different $Alq_3$ devices with ITO, PEDOT:PSS/ITO, and

HB-PES/ITO anodes were 0.176, 0.373, and 1.39 ms, respectively. This is different from what we usually observe in the EL devices in which more balanced electron−hole recombination resulted in faster $t_r$ values.[31] Indeed, we observe the opposite trend that more efficient devices showed slower $t_r$ values. This is because the holes promoted by accumulated electrons give rise to slow EL rise in addition to the original transient EL output, which is supported by Figure 5. Figure 5a shows the transient EL of the three different devices. It should be noted that the device using HB-PES showed an additional slow EL rise after the EL output was first saturated before 20 $\mu$s. The device using PEDOT:PSS also showed a little slower EL rise than the device with bare ITO. The PSS in the PEDOT:PSS complex can be rich at the surface of the PEDOT:PSS film,[5] so the enriched PSS at the surface possess an electron-blocking characteristic in the device. This property results in electron accumulations at the interface, which eventually induces more holes from the anode.[32] The slow current rising phenomena were found from the transient current, as shown in Figure 5b. Indeed, the hole current tends to increase slowly by accumulated electron space charges according to the electron-blocking capability of the hole-injection/electron-blocking buffer layers on the ITO. When the devices are turned off, the accumulated electrons can recombine with the residual holes. Therefore, Figure 5c shows that as accumulated electrons increase, the EL decay can be slower. These EL decay characteristics are also consistent with the transient EL rising data and transient current data as we discussed above.

## Conclusion

We synthesized an organic-soluble hyperbranched poly(ether sulfone) with sulfonic acid terminal. Spin-casting the solution onto ITO provides a homogeneous thin nanolayer with good adhesion. This thin organic buffer layer is advantageous over the conventional PEDOT:PSS, as it can be processed in an inert glovebox and the moisture uptake problem can be avoided. We employed the HB-PES material as a thin hole-injection nanolayer on top of ITO in $Alq_3$-based organic light-emitting diodes to investigate the mechanism of hole-injection and electron-blocking. The hole-injection is facilitated by the enhanced work function of the anode. However, the major role of the layer is electron-blocking at the HB-PES/$Alq_3$ interface. Although the current density of the device is reduced by the electron-blocking of the HB-PES layer, the luminous efficiency turned out to be much better than that of the device using conventional hole-injection layer, PEDOT:PSS. The electron-blocking capability of HB-PES leads to the electrons accumulation at the HB-PES/$Alq_3$ interface. In turn, the accumulated electrons can induce more holes from the ITO anode, which was supported by transient current and EL studies. The additional slow current and EL rise can be ascribed to the additional injection of holes, which is promoted by accumulated charges at the interface of the HB-PES/$Alq_3$. We suggest that the electron-blocking capability should be considered when designing the hole-injection layers in the future, especially in the simplified structure such as solution-processed OLED devices.

(31) Lee, T.-W.; Kim, M.-G.; Kim, S. Y.; Park, S. H.; Kwon, O.; Noh, T.; Oh, T.-S. *Appl. Phys. Lett.* **2006**, *89*, 123505.
(32) Van Woudenbergh, T.; Wildeman, J.; Blom, P. W. M.; Bastiaansen, J. J. A. M.; Langeveld-Voss, B. M. W. *Adv. Funct. Mater.* **2004**, *14*, 677.